Additive Noise for Storm-Scale Ensemble Data Assimilation

DAVID C. DOWELL

National Center for Atmospheric Research, Boulder, Colorado*

LOUIS J. WICKER

NOAA/OAR/National Severe Storms Laboratory, Norman, Oklahoma

(Manuscript received 14 April 2008, in final form 5 September 2008)

ABSTRACT

An ''additive noise'' method for initializing ensemble forecasts of convective storms and maintaining ensemble spread during data assimilation is developed and tested for a simplified numerical cloud model (no radiation, terrain, or surface fluxes) and radar observations of the 8 May 2003 Oklahoma City supercell. Every 5 min during a 90-min data-assimilation window, local perturbations in the wind, temperature, and water-vapor fields are added to each ensemble member where the reflectivity observations indicate precipitation. These perturbations are random but have been smoothed so that they have correlation length scales of a few kilometers. An ensemble Kalman filter technique is used to assimilate Doppler velocity observations into the cloud model. The supercell and other nearby cells that develop in the model are qualitatively similar to those that were observed. Relative to previous storm-scale ensemble methods, the additive-noise technique reduces the number of spurious cells and their negative consequences during the data assimilation. The additive-noise method is designed to maintain ensemble spread within convective storms during long periods of data assimilation, and it adapts to changing storm configurations. It would be straightforward to use this method in a mesoscale model with explicit convection and inhomogeneous storm environments.

1. Introduction

Several recent studies have evaluated ensemble Kalman filter (EnKF) techniques for determining the atmospheric state on the scale of individual convective storms through assimilating radar observations into numerical cloud models (e.g., Snyder and Zhang 2003; Dowell et al. 2004a,b; Caya et al. 2005; Tong and Xue 2005; Aksoy et al. 2009). The EnKF uses the statistics of a forecast ensemble to estimate the background-error covariances needed for data assimilation (Evensen 1994; Houtekamer and Mitchell 1998). Initial tests of the EnKF method for atmospheric data assimilation were for large-scale, quasigeostrophic flows. Snyder and Zhang (2003) later applied the EnKF technique to smaller-scale, unbalanced flows, specifically convective storms.

For ensemble forecasting and data assimilation at any scale, it is difficult to produce an ensemble with statistics that appropriately represent actual forecast uncertainty. For applications that involve short periods of data assimilation, it is challenging to construct an initial ensemble that spans a reasonable subspace of possible atmospheric states and that will promote efficient state estimation as the initial sets of observations are assimilated (Snyder and Zhang 2003; Zhang et al. 2004). More generally, it is challenging to maintain ensemble spread in the appropriate locations and model variables so that the assimilation continues to be successful. Model bias errors, which are pervasive in numerical meteorological prediction (Dee and da Silva 1998), particularly lead to inconsistency between ensemble statistics and forecast errors. Furthermore, assimilating observations typically reduces the ensemble spread too much because covariance estimates from finite-sized ensembles are noisy (Hamill et al. 2001).

* The National Center for Atmospheric Research is sponsored by the National Science Foundation.

Corresponding author address: David C. Dowell, National Center for Atmospheric Research, P. O. Box 3000, Boulder, CO 80307-3000.
E-mail: ddowell@ucar.edu

DOI: 10.1175/2008JTECHA1156.1

Ensemble prediction on the storm scale[1] is a relatively new endeavor, and researchers have just begun to explore some of the possibilities for ensemble design. Since convective storms are localized disturbances that are sampled with incomplete observations, ensemble design is particularly difficult. Nevertheless, some of the ad hoc storm-scale ensemble techniques that have been developed so far have proved to be useful for data assimilation (Snyder and Zhang 2003; Zhang et al. 2004; Dowell et al. 2004a,b; Caya et al. 2005; Tong and Xue 2005). For their ''perfect model'' supercell experiments, Snyder and Zhang (2003) and later Tong and Xue (2005) initialized ensembles with different realizations of random, Gaussian noise added to the idealized base state. Snyder and Zhang added noise throughout the domain to the three velocity components and to the liquid-water potential temperature and then advanced the ensemble 20 min before assimilating the first observations. The subsequent data-assimilation procedure utilized the background-error covariances associated with different realizations of incipient convective storms that had developed within the ensemble during the 20-min integration. Snyder and Zhang (2003) then compared these experiments to a set of experiments in which the initial noise was confined horizontally to a 20 km $\times$ 20 km subdomain centered on the approximate storm location in the reference simulation. They found that the localized noise method was preferable, owing to fewer spurious convective cells within the domain overall.

For EnKF data-assimilation experiments with real radar observations of a supercell, Dowell et al. (2004a) initialized a 50-member ensemble with smooth perturbations rather than gridpoint noise. Ellipsoidal perturbations several kilometers wide and tall were added to the model fields (horizontal wind components, liquid-water potential temperature, rainwater, and total water), and the ensemble was advanced 20 min before the first data assimilation. The initial perturbations were localized around the observed storm location, as suggested by Snyder and Zhang (2003). Dowell et al. (2004a) obtained better results for the initialization with smooth perturbations than for an initialization with gridpoint noise, noting that the smooth perturbations resulted in more rapid updraft development and greater ensemble spread throughout the assimilation period.

Whereas Snyder and Zhang (2003) and Dowell et al. (2004a) manually selected rectangular subdomains for the initial perturbations, Caya et al. (2005) developed a more automated procedure for adding smooth, random, localized perturbations to the initial ensemble. This technique uses high-reflectivity observations as indicators of convective cells and thus locations where perturbations are needed. The Caya et al. technique, described in detail in the following section, is the foundation for the ''additive noise'' method developed in the current study.

The techniques just described mainly concern how to generate the initial ensemble. A relatively unexplored but arguably more important topic in storm-scale ensemble data assimilation is how to maintain ensemble spread during the assimilation, to counteract the tendency for the distribution to converge on a solution different from the truth (Jazwinski 1970; Anderson and Anderson 1999). A common approach for dealing with this problem of filter divergence is to multiply the prior deviations of the ensemble members from the mean by a factor γ (>1) before each observation set is assimilated (Anderson and Anderson 1999; Anderson 2001; Hamill et al. 2001). This technique for artificially broadening the prior distribution is often called ''covariance inflation.'' Experimentation and/or adaptive methods that use recent innovation statistics (e.g., Anderson 2009) are required to determine the inflation factor γ that provides the most favorable results for a particular application.

Attempts to tune the EnKF for storm-scale data assimilation have included constant covariance inflation (Snyder and Zhang 2003; Dowell et al. 2004a; Tong and Xue 2005), but results have been mixed. Snyder and Zhang (2003) found that inflation degraded their results, owing to its enhancement of spurious cells in the ensemble. Dowell et al. (2004a) reported only minor improvement (2% reduction in root-mean-square innovation) through the use of covariance inflation. Another approach for maintaining ensemble spread during storm-scale data assimilation is the ''relaxation'' method of Zhang et al. (2004). This method, which is essentially local inflation, restores a specified fraction of the ensemble spread that was lost when observations were assimilated.

Our goal here is to develop a method for initializing storm-scale ensembles and maintaining ensemble spread throughout periods of data assimilation with the following characteristics: 1) the perturbed regions are selected automatically from observations rather than manually; 2) the perturbations are spatially smooth[2]; 3)

[1] ''Storm-scale'' forecasting refers here to using numerical models with grid spacings ~1 km to predict convective storm features ~10 km wide/tall.

[2] Perturbations that have correlation length scales comparable to those of the simulated convective storms seem physically reasonable and have proven useful in storm-scale data-assimilation experiments (Dowell et al. 2004a).

the perturbation magnitudes are relatively large in and near convective storms and relatively small in the environment far away from the storms; and 4) the method can be applied throughout the assimilation window, rather than just at the beginning. The method we propose is to add random, smooth perturbations to selected model fields at regular intervals throughout the assimilation window in and near convective storms, as identified by high-reflectivity observations. This additive-noise method is similar to that proposed by Caya et al. (2005), except the current method adds perturbations every few minutes throughout the data-assimilation period, rather than only at the initial time when the ensemble is populated.

Additive noise has proven useful for ensemble forecasting and data assimilation at larger scales. Mitchell and Houtekamer (2000) attempted to account for model error in a three-level quasigeostrophic model by estimating parameters in a simple representation of model error and adding random, smooth perturbations to the ensemble members to increase the spread in a manner reflecting the estimated model error. The Mitchell and Houtekamer (2000) technique is adaptive in that the perturbation magnitudes and length scales are based on innovation statistics from the data assimilation. This approach for parameterizing model error was later implemented successfully in an operational global model (Houtekamer and Mitchell 2005). Although there are a number of similarities to the additive-noise technique used in the current study, a key difference is that the perturbations are localized here (in and near convective storms), whereas the model-error parameterization of Houtekamer and Mitchell (2005) has statistics that are horizontally homogeneous.

For data-assimilation and forecasting experiments with a two-layer primitive equation model, Hamill and Whitaker (2005) considered various methods for accounting for model error owing to unresolved scales. They obtained significant improvement in their results by adding spatially smooth random perturbations to each ensemble member. The characteristics of the additive noise were based on samples of model error from a time series of differences between model forecasts at two different resolutions. Hamill and Whitaker (2005) noted that an ensemble modified through additive noise could ''span a somewhat different subspace'' than an unmodified ensemble or an ensemble modified through covariance inflation.

An additive-noise approach for storm-scale ensemble forecasting and data assimilation is demonstrated here for the 8 May 2003 Oklahoma City supercell (Fig. 1) (Dowell et al. 2004b; Romine et al. 2008). For this study, *only Doppler radial-velocity observations* from a 10-cm radar are assimilated into a numerical cloud model. Reflectivity observations are used to determine where noise is added to model fields. Results of experiments with different magnitudes of additive noise are compared. An additive-noise experiment is then compared to experiments initialized as in previous studies (e.g., Dowell et al. 2004a,b). The additive-noise technique is successful in producing and maintaining ensemble spread within the observed convective storms while producing minimal spurious convection.

2. Experiment design

a. Numerical cloud model

The numerical cloud model employed in this study is the National Severe Storms Laboratory (NSSL) Collaborative Model for Multiscale Atmospheric Simulation (NCOMMAS) (Wicker and Skamarock 2002; Coniglio et al. 2006), which is a nonhydrostatic, compressible model designed for simulating convective storms in a simplified setting. Like the Klemp and Wilhelmson (1978) model, NCOMMAS includes the following simplifications: a flat lower boundary, no surface fluxes, no radiative transfer, and a base state that is assumed to be uniform at each vertical level. Although the simplified framework is sufficient for developing and testing the additive-noise technique here, it would also be straightforward to implement the technique in a mesoscale model with full complexity, which would presumably be more suitable for forecasting convective storms.

The prognostic variables in NCOMMAS are u (westerly wind component); v (southerly wind component); w (vertical wind component); π (Exner function); K_m (mixing coefficient); θ (potential temperature); $q_1 = q_v$ (water-vapor mixing ratio); $q_2 = q_c$ (cloud water mixing ratio); and $q_{3\ldots n}$ (hydrometeor mixing ratio), where n, the number of water substance categories, depends on which of several options in NCOMMAS are chosen for the precipitation-microphysics scheme. For this study, we use the Gilmore et al. (2004) version of the Lin et al. (1983) precipitation-microphysics scheme, which is a typical single-moment bulk scheme for cloud modeling. This scheme includes two liquid categories and three ice classes: $q_{2\ldots6} = q_c$ (cloud droplets), q_r (rain), q_i (cloud ice crystals), q_s (snow), and q_h (hail/graupel). The moist processes represented in the model are cloud condensation, cloud and rain evaporation, autoconversion of cloud to rain, ice-crystal initiation, vapor deposition and sublimation for ice species, freezing, melting, accretion, aggregation, rain shedding by wet hail/graupel, and precipitation fallout (Gilmore et al. 2004). The cloud water and ice-crystal distributions in the model are monodispersed,

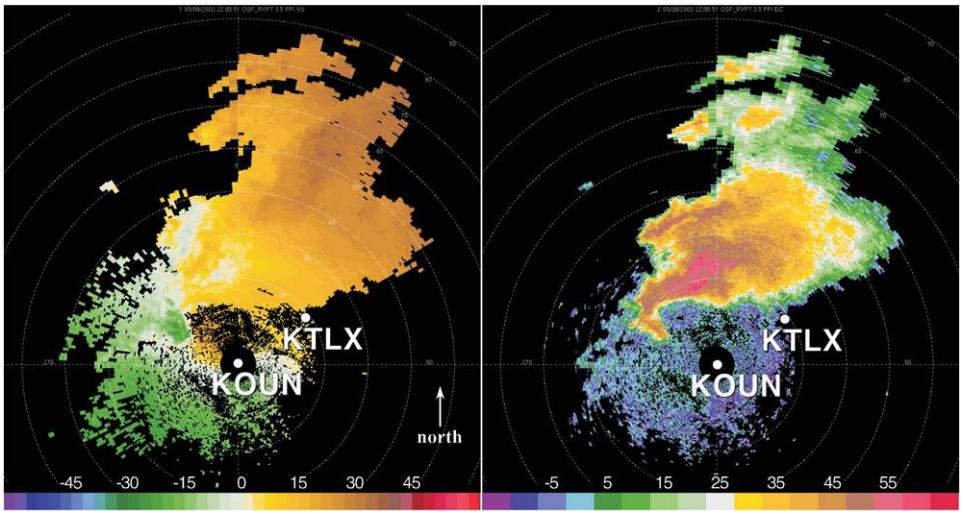

FIG. 1. (left) Doppler velocity (m s^{-1}) and (right) effective reflectivity factor (dBZ) from the KOUN radar at 3.5° elevation angle at 2205 UTC 8 May 2003. Range rings are every 10 km. The locations of the KOUN and KTLX radars are shown.

whereas the rain, snow, and hail/graupel categories have inverse exponential distributions. For this study, the intercept parameters for the rain and hail/graupel size distributions are 8.0×10^6 and 4.0×10^4 m^{-4}, respectively, and the hail density is 900 kg m^{-3} (Gilmore et al. 2004).

For our experiments with the 8 May 2003 Oklahoma City supercell (Fig. 1), the model domain is 100 km wide in both horizontal directions, is 18 km tall, and moves at $U = 14$ m s^{-1}, $V = 8$ m s^{-1}, following the storm of interest. The constant grid spacing is 1.0 km (0.5 km) in the horizontal (vertical) coordinate. The boundary conditions for the simulations are free slip at the top and bottom, and the lateral boundaries are open and permeable. The prognostic equations are advanced with third-order Runge–Kutta time integration and fifth- (third-) order horizontal (vertical) spatial differencing (Wicker and Skamarock 2002). Other model details are described by Coniglio et al. (2006). We do not include a Coriolis force in our simulations. The initial background u, v, θ, and q_v profiles in the raw 0000 UTC 9 May 2003 Norman, Oklahoma, sounding (Fig. 3 of Romine et al. 2008) are interpolated to model grid levels in order to initialize the base state in the model (Fig. 2). The model time step is 5 s, which is sufficient to maintain computational stability.[3]

[3] While a larger time step would generally be permissible for simulations with the given grid spacing and flow parameters, our data-assimilation experiments have often become unstable when a larger time step is used. The numerical instability appears to occur near storm top, where the data assimilation results in significant local deviations from anelastic incompressibility.

b. Data assimilation

The test case for this study is the 8 May 2003 supercell that produced a violent tornado in Oklahoma City (Burgess 2004; Dowell et al. 2004b; Romine et al. 2008). Observations of this storm are available from multiple radars, including the KOUN radar (a 10-cm prototype dual-polarization radar in Norman, Oklahoma) and the KTLX radar [the operational Weather Surveillance Radar-1988 Doppler (WSR-88D) southeast of Oklahoma City] (Fig. 1). Only Doppler velocity observations from KOUN are assimilated into NCOMMAS in this study; reflectivity from KOUN and Doppler velocity from KTLX are used for verification.

The KOUN radar obtained volumetric scans (14 different elevation angles) of the Oklahoma City supercell approximately every 6 min, including the period of interest in the current study from "first echoes" of the Oklahoma City storm at 2046 UTC to the beginning of the tornadic phase at 2210 UTC. The Doppler velocity data that are assimilated into NCOMMAS have been edited manually (which involves unfolding aliased Doppler velocities and removing ground clutter, range folding, and other spurious data) and objectively analyzed. The quality-controlled observations are located in precipitation regions throughout the domain and in "clear air" at low levels relatively close to the radar (Fig. 1). We objectively analyze each radar sweep separately to grid points on the conical scan surfaces (Sun and Crook 2001; Dowell et al. 2004a). The grid points are 2000 m apart in each horizontal direction, and the radius of influence for the Cressman objective analysis is 1000 m. The grid spacing for the objective analysis is

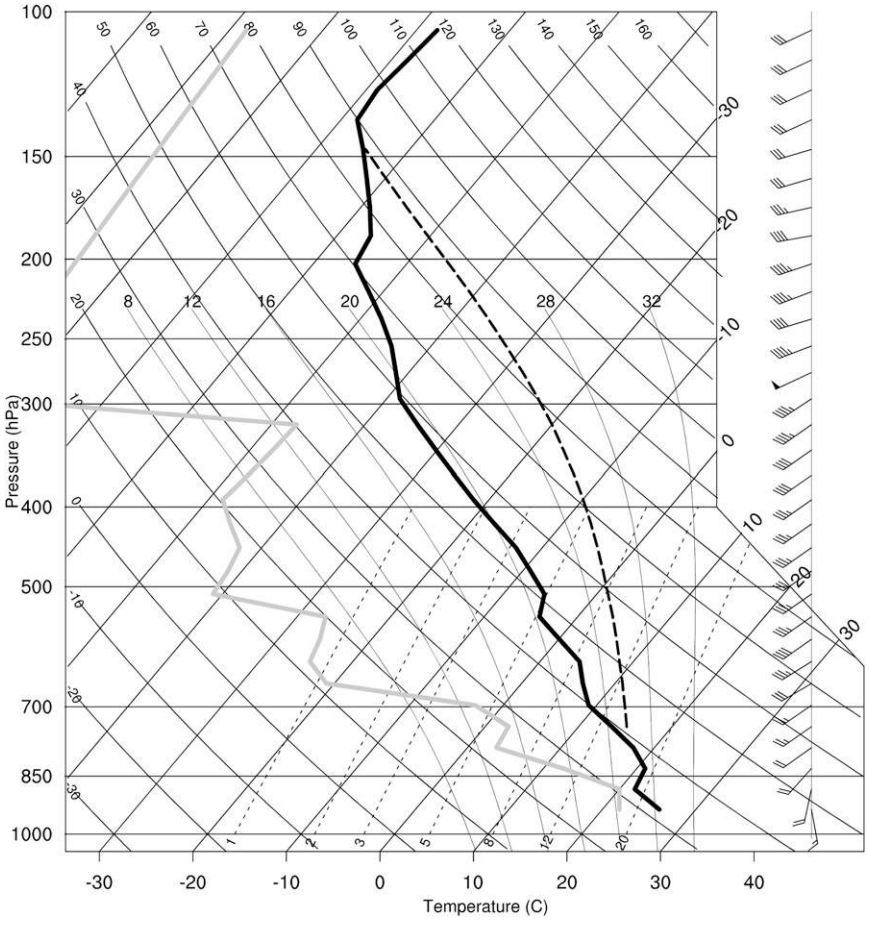

FIG. 2. Skew T–log p diagram for the base state in the assimilation experiments, obtained by interpolating the 0000 UTC 9 May 2003 Norman, OK, sounding to model grid levels. The solid black and gray lines indicate the temperature and dewpoint profiles, respectively. The dashed line indicates temperature for a lifted surface parcel. Wind barbs (flags) represent 10 m s^{-1} (50 m s^{-1}).

roughly the same as the mean observation spacing for the more distant radar observations.

The data-assimilation experiments proceed as follows: 1) create an initial ensemble of model states; 2) advance the ensemble to the first observation time; 3) assimilate all observations within 60 s of the current time; 4) advance the ensemble 60 s, or to the time of the next observation that has not yet been assimilated, whichever is later; and 5) repeat steps 3 and 4 until all observations have been assimilated. For the Oklahoma City supercell case, the number of Doppler velocity observations assimilated during each 60-s period ranges from 100 to 5500, depending on the current number of convective storms, their sizes, and the heights of the radar scans.

The EnKF method we use to assimilate observations [described in more detail by (Dowell et al. 2004a)] is commonly called an ensemble square root filter (EnSRF) (Whitaker and Hamill 2002). Each time an observation is assimilated, the ensemble mean and members are updated according to the following equations:

$$K = \frac{\frac{1}{N-1}\sum_{n=1}^{N}(x_n^f - \bar{x}^f)[H(\mathbf{x}_n^f) - \overline{H(\mathbf{x}^f)}]}{\sigma^2 + \frac{1}{N-1}\sum_{n=1}^{N}[H(\mathbf{x}_n^f) - \overline{H(\mathbf{x}^f)}]^2}, \quad (2.1)$$

$$\beta = \left[1 + \sqrt{\frac{\sigma^2}{\sigma^2 + \frac{1}{N-1}\sum_{n=1}^{N}[H(\mathbf{x}_n^f) - \overline{H(\mathbf{x}^f)}]^2}}\right]^{-1}, \quad (2.2)^4$$

[4] The corresponding equation in Dowell et al. (2004a) contains an error (a missing square root symbol).

$$\bar{x}^a = \bar{x}^f + WK[\,y^o - \overline{H(\mathbf{x}^f)}], \tag{2.3}$$

$$x_n^a = \bar{x}^a + (x_n^f - \bar{x}^f) + WK\beta[\overline{H(\mathbf{x}^f)} - H(\mathbf{x}_n^f)], \tag{2.4}$$

where K is the Kalman gain; N is the number of ensemble members (50 in our experiments); n is an index that identifies a particular ensemble member; x represents a particular model field at a particular grid point; $\mathbf{x}$ represents the entire model state; superscript f indicates a prior estimate (i.e., before the observation is assimilated); superscript a indicates an analysis estimate (i.e., after the observation is assimilated); an overbar indicates an ensemble mean; H is the observation operator, which maps the model state to the observation type and location; σ^2 is the observation-error variance [assumed to be $(2.0\ \text{m}\ \text{s}^{-1})^2$ for Doppler velocity observations in our experiments, as in Dowell et al. (2004a)]; β is the reduced-gain factor (Whitaker and Hamill 2002); y^o is the observation; and W is a localization factor (Houtekamer and Mitchell 2001), which decreases from 1 at the observation location to 0 at and beyond a specified distance from the observation. Observations are assimilated serially (one after the other), which is an approximation based on an assumption that observation errors are uncorrelated in space and time. We use trilinear interpolation to compute point estimates of model fields at observation locations. Thus, the H operator approximates the method used to objectively analyze the observations.

The functional form of W is taken from the compactly supported fifth-order correlation function in Eq. (4.10) of Gaspari and Cohn (1999). We specified 6 km as the radius (same in horizontal and vertical directions) at which $W = 0$; this choice follows Dowell et al. (2004a) and was confirmed through experimentation as appropriate for the current study. Assimilating an observation involves computing the Kalman gain and reduction factor [Eqs. (2.1) and (2.2)], updating the ensemble mean [Eq. (2.3)], and then updating each ensemble member [Eq. (2.4)] for each model variable at each grid point within 6 km of the observation. After the current observation is assimilated, the analysis state estimate becomes the new prior state estimate before the next observation is assimilated with the same procedure.

During the early stages of this work, we noticed that we obtained comparable assimilation results whether the filter was allowed to update π and K_m or not. Therefore, to reduce computing time, we do not update these variables when assimilating observations. All other model variables are updated by the filter. Positive definite model variables (q_1,...,q_6) are immediately reset to zero if they become negative during the data assimilation.

c. Ensemble initialization and additive noise

The perturbation procedure for each ensemble member and each model field begins with an array that contains Gaussian noise in high-reflectivity regions and is zero elsewhere:

$$f'(i, j, k) = \begin{cases} N(0, \sigma_f^2), & \text{if } Z_{\text{dB}}(i, j, k) \geq Z_{\min} \\ 0, & \text{otherwise} \end{cases}, \tag{2.5}$$

where f' is a perturbation array; i, j, and k are model grid indices in the X (eastward), Y (northward), and Z (upward) directions, respectively; $N(0, \sigma_f^2)$ is a Gaussian random variable with mean 0 and variance σ_f^2; Z_{dB} is the observed reflectivity (more precisely, the effective reflectivity factor in dBZ); and $Z_{\min}$ is a reflectivity threshold. A different realization of the perturbation array f' is produced for each ensemble member and for each perturbed model variable. The primary motivation for adding perturbations in and near high-reflectivity regions only is that these observations indicate where the intense, localized disturbances associated with convective storms are present. In addition, introducing perturbations in precipitation regions counteracts the tendency for ensemble spread to become too low where plentiful observations are assimilated; dense coverage of both Doppler velocity and reflectivity observations is typically available in precipitation regions (e.g., Fig. 1).

The Z_{dB} array needed in Eq. (2.5) is obtained by mapping recent reflectivity observations to the nearest model grid points. For our experiments with the Oklahoma City supercell, the ensemble of model states is perturbed every 5 min, and thus the gridded Z_{dB} values at the current time are produced from all observations available during the preceding 5 min. If there are no recent reflectivity observations near a model grid point, at that point Z_{dB} is assigned a value below the $Z_{\min}$ threshold. The threshold reflectivity for our supercell experiments is $Z_{\min} = 20$ dBZ, which excludes "clear air" (nonprecipitation observations) and includes most precipitation regions.

The second step in the perturbation procedure is to smooth the perturbation array f' while it is added to the model field (Caya et al. 2005):

$$f^{\text{perturbed}}(l, m, n) = f^{\text{unperturbed}}(l, m, n) + \sum_{i,j,k} f'(i, j, k) \quad \exp\left(-\frac{|X_i - X_l|}{l_h} - \frac{|Y_j - Y_m|}{l_h} - \frac{|Z_k - Z_n|}{l_v}\right), \tag{2.6}$$

where f is a model field before and after perturbation; l, m, and n are model grid indices; and l_h and l_v are horizontal and vertical length scales for the smoothed perturbations, respectively. Following Caya et al. (2005), we choose $l_h = 4$ km and $l_v = 2$ km for the length scales.

Each model field for each of the 50 ensemble members is perturbed independently. Equation (2.6) spreads the localized noise generated by Eq. (2.5) to surrounding points in a smooth manner. The smoothing function (from Caya et al. 2005) is computationally expensive, but the contribution of the perturbation procedure to the total time for an assimilation experiment is small if parallel processing is used. More computationally efficient approaches for generating spatially correlated noise with spatially varying variance are also possible and should produce comparable results.

The additive-noise technique allows one to select what model variables are perturbed, by how much, and how often. For the current study, we adopt a conservative approach of perturbing only a subset of the model variables (specifically, the same set of model variables that defined the original model base state): u, v, θ, and q_v. Selecting appropriate values for the perturbation magnitudes (σ_f) requires experimentation; results for various choices are shown in section 3. We use a 5-min interval between applications of the perturbation procedure, which means that perturbations are introduced several times during the life cycle of a typical convective cloud.

To perturb water vapor, we temporarily transform the model fields to dewpoint temperature T_d (Fujita et al. 2007). Through such a transformation, complications associated with the nonnegative nature of q_v are avoided. A uniform standard deviation for the random T_d perturbations is used throughout the domain. After the reverse transformation, the resulting q_v perturbations are relatively large where q_v is large and relatively small where q_v is small.

Figure 3 shows an example of perturbations produced through Eqs. (2.5) and (2.6) for a volume of reflectivity observations during the early development of the Oklahoma City supercell. The standard deviations of random noise (before smoothing) were 1.0 K and 1.0 m s^{-1} for the potential temperature field and the horizontal wind components, respectively. Prominent features in the smoothed temperature and wind perturbations are several kilometers wide, have magnitudes of several K and m s^{-1}, and are localized near the precipitation cores.

3. Observation-space diagnostics for additive-noise experiments

Sensitivities of the data-assimilation results to the magnitudes of additive noise are considered in the first set of experiments. In all experiments, relatively large perturbations are added during the first 20 min, and then smaller perturbations (of different magnitudes for different experiments) are added for the remainder of the assimilation window. The large initial perturbations help initiate convective storms in the ensemble, at a time when large ensemble spread is needed to reflect large uncertainty in the atmospheric state. All experiments are initialized at 2040 UTC with additive noise based on reflectivity observations in the first KOUN radar volume (2046–2052 UTC). Using observations at a slightly later time to influence the initialization in these experiments is analogous to the approach in previous studies of confining initial perturbations to a subdomain upstream of future convective cells (e.g., Snyder and Zhang 2003; Dowell et al. 2004a). For the remainder of the assimilation window, the additive noise every 5 min is based on reflectivity observations available during the *preceding* 5 min. For all five experiments, the standard deviations (σ_f) of random noise, before smoothing, are 1.0 m s^{-1}, 1.0 m s^{-1}, 1.0 K, and 1.0 K for u, v, θ, and T_d, respectively, between 2040 and 2100 UTC. The random number generator for the additive noise is seeded with the same value in all five experiments, so results are identical until 2100 UTC (Fig. 4). After 2100 UTC, the perturbation magnitudes in the different experiments (hereafter the "0.75," "0.50," "0.25," "0.10," and "0.00" experiments) range from 0.75 m s^{-1}, 0.75 m s^{-1}, 0.75 K, and 0.75 K to 0.00 m s^{-1}, 0.00 m s^{-1}, 0.00 K, and 0.00 K. Experiments with perturbations larger than 0.75 m s^{-1} and 0.75 K after 2100 UTC have worse results than the 0.75 experiment, and thus these additional results are not shown.

The analysis and forecast summary statistics in Figs. 4, 5, 6a, and 7 are for the KOUN Doppler velocity observations (the assimilated observations), averaged over each radar volume (i.e., over periods of approximately 6 min). Since our study focuses on optimizing ensemble spread and minimizing forecast and analysis error near the convective storms, we only include locations where the observed reflectivity exceeds 15 dBZ in the statistical computations (similar to Snyder and Zhang 2003 and Tong and Xue 2005). Three basic quantities are computed: the volume-mean innovation $\langle d \rangle$, where

$$d = y^o - \overline{H(\mathbf{x}^f)} \quad \text{or} \quad y^o - \overline{H(\mathbf{x}^a)}, \tag{3.1}$$

and brackets indicate an average over all observations in a radar volume; the root-mean-square of the innovations (with the volume mean removed),

$$\text{RMSI} = \sqrt{\langle (d - \langle d \rangle)^2 \rangle}; \tag{3.2}$$

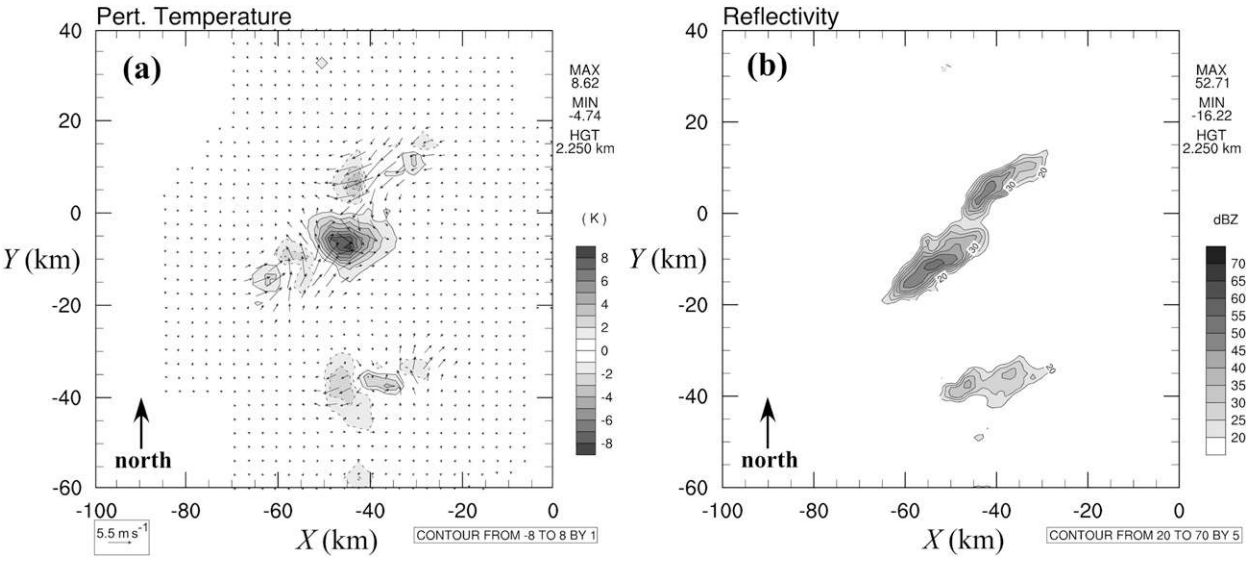

FIG. 3. (a) Example of random perturbations in potential temperature (contours and shading at intervals of 1.0 K, with dashed contours for negative values) and horizontal wind (vectors) added to an ensemble member at 2.25 km AGL. (b) The corresponding reflectivity observations from KOUN (contours and shading at intervals of 5 dBZ). The X and Y coordinates (km) are relative to KOUN.

and a measure of the ensemble spread that includes the observation error,

$$\text{spread} = \sqrt{\sigma_{\text{vr}}^2 + \left\langle \frac{1}{N-1}\sum_{n=1}^{N}[H(\mathbf{x}_n) - \overline{H(\mathbf{x})}]^2 \right\rangle}, \quad (3.3)$$

where σ_{vr} is assumed to be 2.0 m s^{-1} in these experiments (Dowell et al. 2004a).

A favorable decrease with time in forecast volume-mean innovation is indicated in all experiments (Fig. 4). The least favorable results (largest forecast RMSI and often the largest forecast volume-mean innovation) are obtained in the 0.00 and 0.10 experiments, which have no or relatively little additive noise after 2100 UTC. The results for the other experiments (0.25, 0.50, and 0.75) are comparable in terms of RMSI.

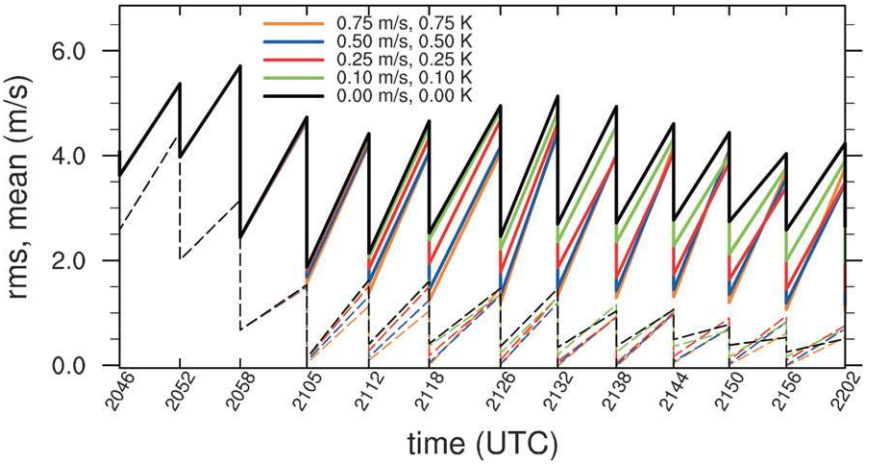

FIG. 4. Observation-space diagnostic statistics for experiments with various magnitudes of additive noise. Each color represents a different standard deviation (σ_f) of random noise after 2100 UTC, ranging from 0.0 m s^{-1} and 0.0 K (black) to 0.75 m s^{-1} and 0.75 K (orange) for (u and v) and (θ and T_d), respectively. The volume-mean innovation $\langle d \rangle$ (dashed lines) and RMSI (solid lines) are computed for KOUN Doppler velocity at locations where the observed reflectivity exceeds 15 dBZ. Results are averaged over each radar volume. Both forecast and analysis statistics are plotted, hence the sawtooth pattern.

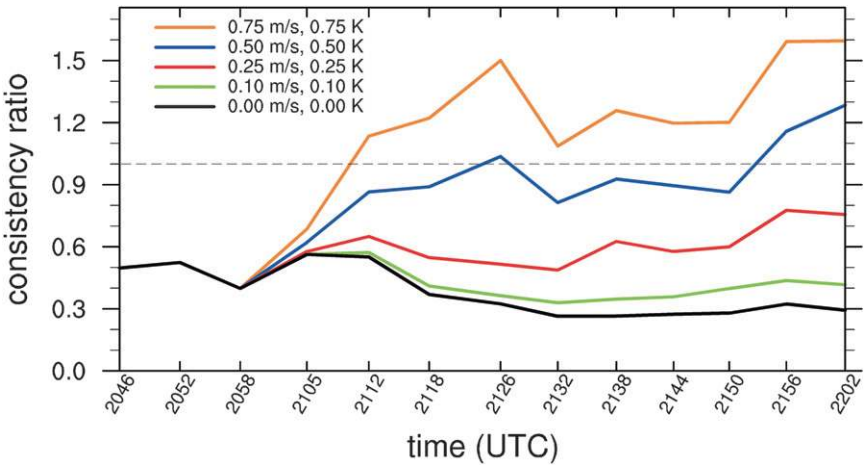

FIG. 5. Consistency ratio [as defined in Eq. (3.4)] for experiments with the different magnitudes of additive noise defined for Fig. 4.

For successful data assimilation, ensemble statistics should be representative of forecast errors. For real data experiments, in which the true forecast errors are unknown and the observations have errors, one can still test whether the spread and RMSI are consistent for the assumed amount of observation error:

$$\text{consistency ratio} = \frac{\sigma_{\text{vr}}^2 + \left\langle \frac{1}{N-1}\sum_{n=1}^{N}[H(\mathbf{x}_n^f) - \overline{H(\mathbf{x}^f)}]^2 \right\rangle}{\langle (d - \langle d \rangle)^2 \rangle}, \tag{3.4}$$

which should be approximately 1.0 (Dowell et al. 2004a). In the 0.00 and 0.10 experiments, the consistency ratios range from 0.26 to 0.57 (Fig. 5), suggesting too little ensemble spread in these experiments (and/or an assumed standard deviation of observation errors that is too small). Without additive noise after 2100 UTC in the 0.00 experiment, the consistency ratio decreases with time, which is the same problem observed in another supercell case study (Dowell et al. 2004a) in which no perturbations were added after the initialization time. In contrast, in the 0.75 experiment, the consistency ratio increases with time, reaching values as large as 1.60. Most likely, the magnitude of additive noise is too large in this experiment. The 0.25 and 0.50 experiments maintain more favorable consistency ratios (between 0.49 and 1.28 after 2100 UTC). With the limited information available for forecast verification, it is challenging to determine if one of these experiments is better than the other. For the remaining discussion, we choose the 0.25 experiment for comparison to other experiments.

4. Comparison of an additive-noise experiment to other experiments

a. *Observation-space diagnostics*

For comparison to the "additive noise" (0.25) experiment (cf. section 3), two additional radar-data-assimilation experiments, designed like those in previous studies, are conducted for the 8 May 2003 supercell (Table 1). Both of these additional experiments are initialized at 2026 UTC, 20 min before the first observations are assimilated (Snyder and Zhang 2003; Dowell et al. 2004a,b). (Since both Snyder and Zhang and Dowell et al. were attempting to "spin up" convective storms quickly in the ensemble through a short period of radar data assimilation, they found the 20-min period of storm development before the first observations were assimilated helpful.) As in Dowell et al. (2004b), warm bubbles (5-K maximum temperature perturbation, 7.5-km horizontal radius, 2.5-km vertical radius) are added in random locations with centers between 0.25 and 2.25 km AGL and within a 50-km-wide subdomain centered at $X = -80$ and $Y = -30$, just upstream of where the Oklahoma City storm formed. These perturbations produce incipient convective storms in the ensemble during the 20-min integration.

In one of these two "bubbles" experiments, there is no source of ensemble variability other than model processes after the initialization time (Table 1). In the other experiment ("bubbles + inflation"), domainwide prior covariance inflation is applied every time a set of observations is assimilated (every 60 s or more). The selected inflation factor is $\gamma = 1.04$, determined through experimentation to give the most favorable statistics for verification with KOUN and KTLX Doppler velocity observations.

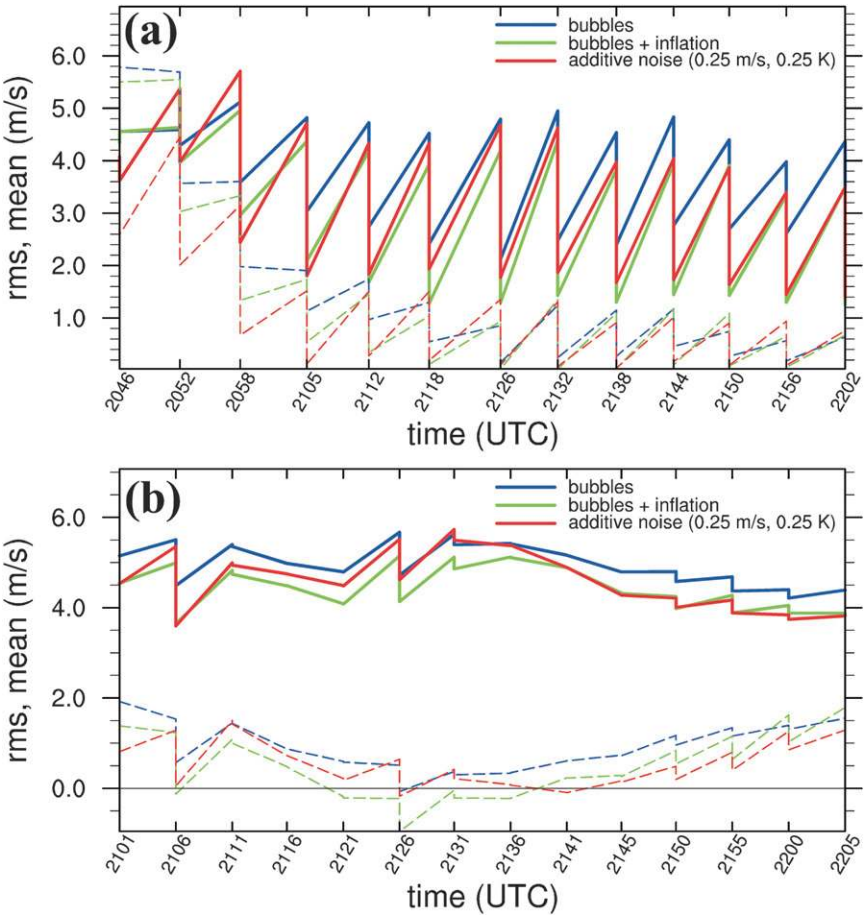

FIG. 6. As in Fig. 4, except for the experiment initialized with warm bubbles at 2026 UTC (blue), the experiment initialized with warm bubbles and with covariance inflation throughout the assimilation window (green), and the experiment initialized at 2040 UTC and with additive noise (0.25 m s^{-1} and 0.25 K) throughout the assimilation window (red). Statistics are computed for Doppler velocity observations from the (a) KOUN radar (the assimilated observations) and (b) KTLX radar (not assimilated) where observed reflectivity exceeds 15 dB*Z*.

Since the additive-noise experiment is initialized 14 min later than the bubbles experiments (Table 1), the results during the first few tens of minutes are not directly comparable. Indeed, the verification statistics for the KOUN observations that are assimilated and the independent KTLX observations show early fluctuations in relative performance for the bubbles, bubbles + inflation, and additive-noise (0.25) experiments as the ensembles adjust to the observations in the first few radar volumes (Fig. 6). Instead, we are more interested in how the statistics evolve in data-assimilation systems that are cycled for long periods of time. After about 2130 UTC, the bubbles experiment has the least favorable statistics overall and is apparently deficient in ensemble spread, as indicated by a consistency ratio much less than 1.0 (Fig. 7). Between 2115 and 2135 UTC, the bubbles + inflation experiment has lower RMSI than the additive-noise (0.25) experiment (Fig. 6). The former experiment could have an advantage from its earlier initialization (cf. Table 1), since the convective cells in the ensemble would mature earlier, possibly leading to more efficient state estimation. After 2135 UTC, the RMSI (Fig. 6) and consistency ratios (Fig. 7) for the bubbles + inflation and additive-noise (0.25) experiments are similar. Based on this performance measure, one might conclude that assimilation success is comparable in these two experiments. Interestingly, the additive noise experiment obtains similar RMSI with a lower consistency ratio (less ensemble spread) than in the bubbles + inflation experiment.

b. Model-space diagnostics

Differences among the experiments are perhaps better revealed by comparing model-space fields. One field

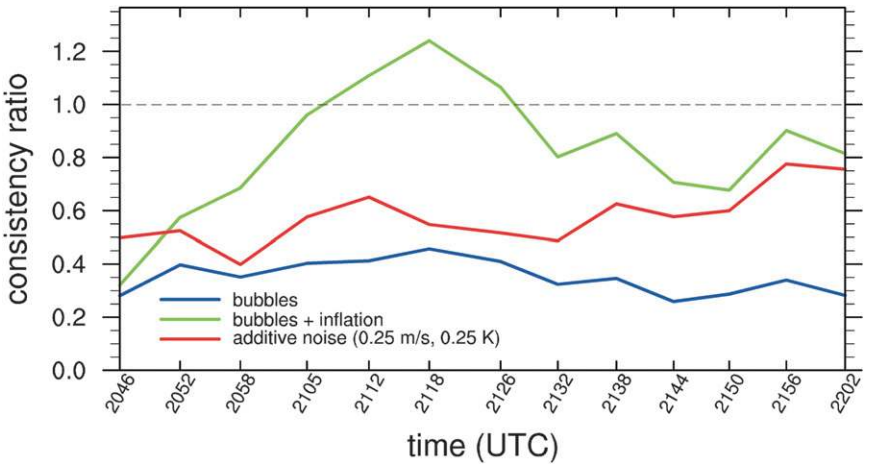

FIG. 7. As in Fig. 5, except for the experiment initialized with warm bubbles at 2026 UTC (blue), the experiment initialized with warm bubbles and with covariance inflation throughout the assimilation window (green), and the experiment initialized at 2040 UTC and with additive noise (0.25 m s^{-1} and 0.25 K) throughout the assimilation window (red).

we use for qualitative verification is the effective reflectivity factor (Fig. 8), an overall indicator of where convective cells are present. (As a reminder, we note that in our experiments, reflectivity observations are used to determine where noise is added to the model fields but are not actually assimilated into the model.) Reflectivity calculations from the model prognostic fields are based on Smith et al. (1975) and Smith (1984); similar equations are used in the study by Tong and Xue (2005). During the early development of the Oklahoma City storm, multiple reflectivity cores formed along a southwest–northeast oriented line (from $X = -70$, $Y = -25$ to $X = -35$, $Y = 10$ in Fig. 8a). These early convective cells are captured in the ensemble mean in the bubbles experiment (Fig. 8b), but numerous spurious convective cells are also produced in the model. The square shape of the subdomain in which warm bubbles are added at 2026 UTC is still apparent at 2100 UTC. The artifacts of this initialization method (also discussed by Snyder and Zhang 2003) were a motivating factor for Caya et al. (2005) to develop an initialization method that introduces perturbations only near observed precipitation. In the current experiments, the spurious cells eventually weaken, owing to strong convective inhibition in the base state (Fig. 2, which shows a relatively stable layer near 850 mb). In other cases, the environment could permit deep, moist convection more readily, and the spurious cells could strengthen and/or grow upscale (Aksoy et al. 2009). Assimilating low-reflectivity (nonprecipitation) observations in the storm environment, which was not attempted here, could suppress the spurious cells (Dowell et al. 2004a; Tong and Xue 2005; Aksoy et al. 2009). Nevertheless, it would be preferable to minimize the introduction of spurious cells in the first place.

By 2208 UTC, when the Oklahoma City supercell was becoming tornadic, all three experiments produce a strong supercell with classic reflectivity structure

TABLE 1. The 8 May 2003 radar-data-assimilation experiments with different methods for populating the initial ensemble and maintaining ensemble spread.

Experiment name	Initialization time (UTC 8 May 2003)	Method for populating initial ensemble	Sources of ensemble spread after initialization time
Additive noise (0.25)	2040	Additive noise*	Model processes, additive noise*
Bubbles	2026	5-K warm bubbles**	Model processes
Bubbles + inflation	2026	5-K warm bubbles**	Model processes, 4% prior inflation

* The standard deviations of random noise, before smoothing, are 1.0 m s^{-1}, 1.0 m s^{-1}, 1.0 K, and 1.0 K for u, v, θ, and T_d, respectively, between 2040 and 2100 UTC, and 0.25 m s^{-1}, 0.25 m s^{-1}, 0.25 K, and 0.25 K after 2100 UTC (cf. sections 2 and 3). Perturbations are added every 5 min.

** The warm bubbles added at 2026 UTC are randomly distributed between 0.25 and 2.25 km AGL and within a 50-km-wide region centered at $X = -80$ km, $Y = -30$ km.

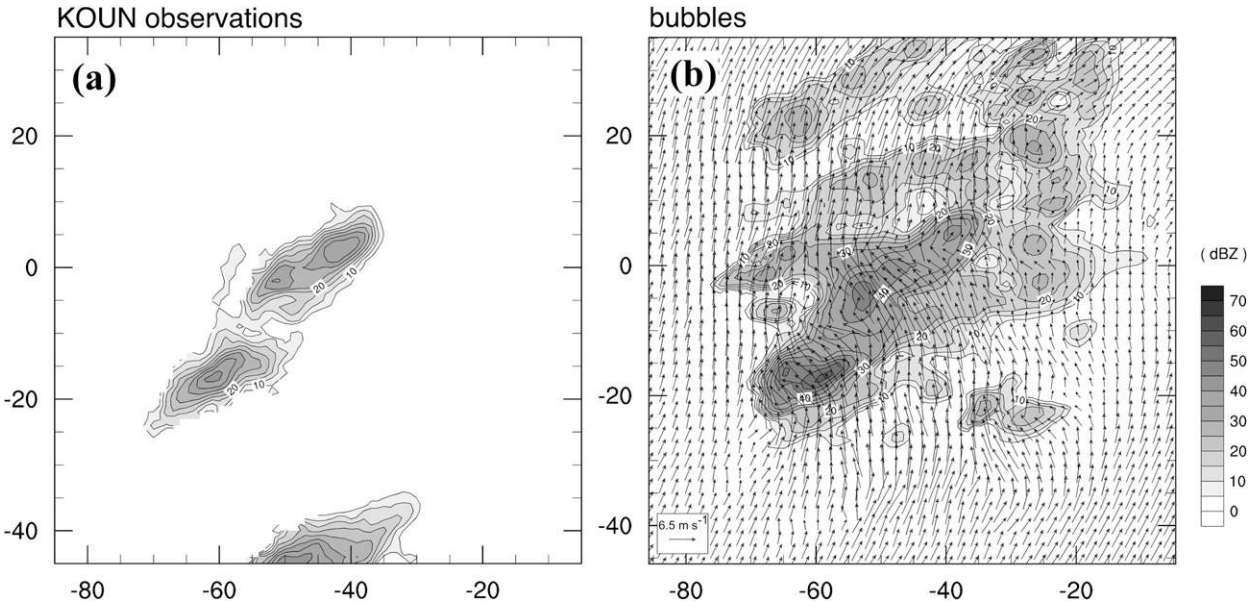

FIG. 8. Effective reflectivity factor (contours and shading at intervals of 5 dBZ) at 1750 m AGL at 2100 UTC. (a) Observations from the KOUN radar. (b) Ensemble mean in the experiment initialized with warm bubbles at 2026 UTC. Horizontal wind vectors are also shown.

(Browning 1964; Lemon and Doswell 1979) in the ensemble mean (Fig. 9). Some of the more obvious differences among the experiments are found north of the supercell. The bubbles experiment (Fig. 9c) most poorly represents the smaller convective cells north of the supercell. The inability of the model to produce these cells through the assimilation of Doppler velocity observations is probably related to insufficient ensemble spread (and thus a low consistency ratio; cf. Fig. 7). The additive-noise and bubbles + inflation experiments both capture the convective cells on the left flank of the supercell (Figs. 9b and 9d). Qualitatively, the reflectivity pattern in the former experiment resembles the observed pattern slightly better than does the latter experiment.

The additive-noise and bubbles + inflation experiments have similar cold pools associated with the supercell (roughly $X = -25$ to 5, $Y = 5$ to 30 in Fig. 10), and the minimum temperature perturbation of -6 K in each experiment agrees with observations (Figs. 4 and 5 of Romine et al. 2008). However, the bubbles + inflation experiment also includes a more widespread cold pool throughout the northwest part of the domain (Fig. 10b). This large spurious cold pool is produced through evaporative cooling in precipitation in the spurious cells that develop from the initial warm bubbles, which persist longer through covariance inflation than they otherwise would. (There is still some evidence of spurious convective cells lingering in the bubbles + inflation experiment at 2208 UTC, e.g., in the northwest corner of Fig. 9d). Even though most of the spurious cells have weakened by 2208 UTC, their cumulative negative effects on the ensemble mean in the bubbles + inflation experiment have been significant. In contrast, the additive-noise technique produces fewer spurious cells and much less evaporatively cooled air at low levels away from the supercell (Fig. 10a).

Patterns in ensemble spread differ greatly among the experiments (Fig. 11). One of our goals (cf. section 1) was to produce relatively large spread among the ensemble members in and near the convective storms and relatively small spread farther away. This goal has been achieved for the additive-noise experiment (Fig. 11a). Significant variability in the v wind component (and other fields; not shown) among the ensemble members is maintained throughout the supercell and the other convective cells to its north. Also, in the storm environment, the region southeast of the supercell inherits ensemble spread from the perturbations added earlier in convective cells southeast of the supercell (Fig. 8). Like the additive-noise experiment, the bubbles experiment at 2208 UTC (Fig. 11b) has relatively large ensemble spread in v centered around $X = 0$, $Y = 25$, which is north of the mesocyclone and in the heart of the precipitation core (Fig. 9). However, the ensemble spread elsewhere is relatively small in the bubbles experiment, and this experiment was shown earlier to have too little spread in wind (Fig. 7).

The bubbles + inflation experiment (Fig. 11c) is much different from the others, developing the greatest

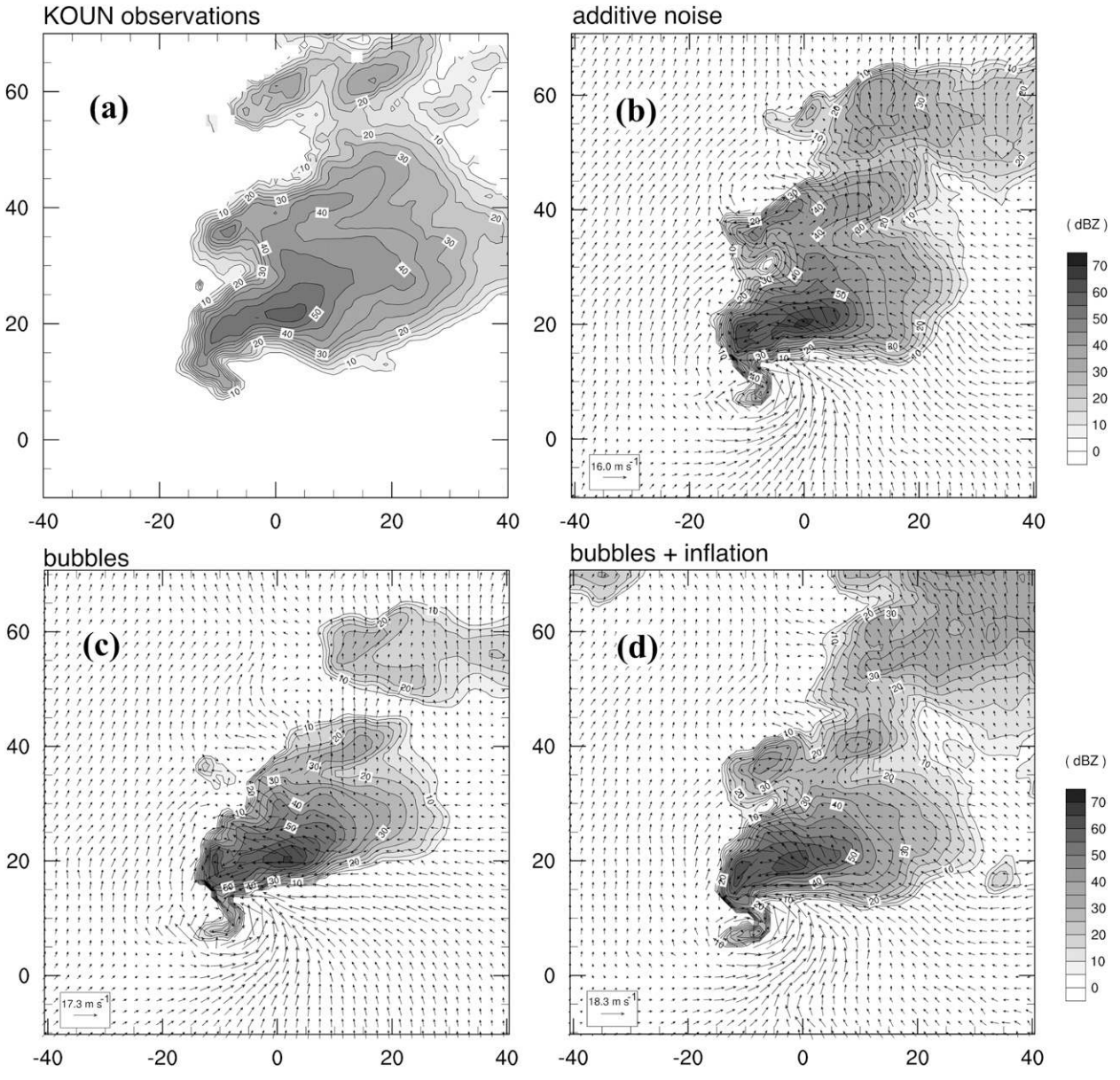

FIG. 9. Effective reflectivity factor (contours and shading at intervals of 5 dBZ) at 1750 m AGL at 2208 UTC. (a) Observations from the KOUN radar. (b) Ensemble mean in the experiment with additive noise (0.25 m s^{-1} and 0.25 K) throughout the assimilation window. Horizontal wind vectors are also shown. (c) Ensemble mean in the experiment initialized with warm bubbles. (d) Ensemble mean in the experiment initialized with warm bubbles and with covariance inflation throughout the assimilation window.

ensemble spread in wind (and other model variables; not shown) in the environment far away from the supercell. Since the designs of the bubbles and bubbles + inflation experiments are the same except for the inflation, the differences in Figs. 11b and 11c illustrate the large impact that repeated covariance inflation has in the environment. The large environmental variability comes from inflation of perturbations associated with spurious cells, gravity waves, etc. While state uncertainty could actually be large in the poorly observed storm environment, we suggest that it would be more realistic to use instead mesoscale and global ensemble techniques (e.g., Stensrud et al. 1999; Buizza et al. 2005; Eckel and Mass 2005) to represent processes leading to environmental variability and to account for model error.

5. Conclusions

An additive-noise method for initializing storm-scale ensembles and maintaining ensemble spread during an assimilation window was developed and tested for

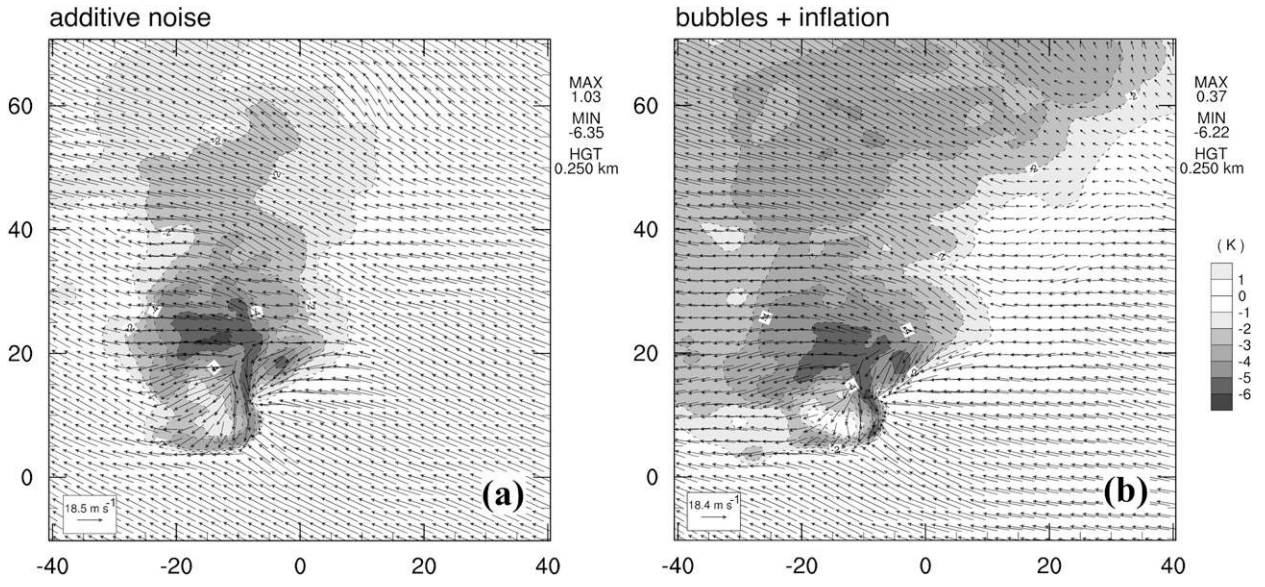

FIG. 10. Ensemble mean perturbation temperature (contours and shading at intervals of 1 K) and horizontal wind (vectors) at 250 m AGL at 2208 UTC. (a) Experiment initialized at 2040 UTC and with additive noise (0.25 m s^{-1} and 0.25 K) throughout the assimilation window. (b) Experiment initialized with warm bubbles at 2026 UTC and with covariance inflation throughout the assimilation window.

Doppler velocity observations of a supercell thunderstorm. Essentially, the method proposed by Caya et al. (2005) for initializing an ensemble with random, smooth perturbations in high-reflectivity regions is applied throughout the assimilation window. An EnKF technique was used to assimilate Doppler velocity observations of the 8 May 2003 Oklahoma City supercell into a numerical cloud model, and u, v, θ, and q_v perturbations were added to the ensemble every 5 min where the reflectivity observations indicated precipitation during the preceding 5 min.

A data-assimilation experiment employing additive noise was compared to more traditional experiments initialized with random perturbations within a subdomain, with or without covariance inflation during the assimilation window. The additive-noise technique was useful for the intended purpose—maintaining significant ensemble spread within the convective storms while leaving the environment relatively undisturbed. In contrast, the experiment with perturbations added only at the initial time became deficient in spread, while the experiment with initial bubbles plus covariance inflation developed large ensemble spread in the environment far away from the storms. All experiments produced a strong supercell in the ensemble mean, but the additive-noise technique had fewer spurious cells and did not generate a large, strong spurious cold pool like that in the bubbles + inflation experiment.

As do experiments with inflation, experiments with the additive-noise method require tuning to produce ensemble spread consistent with innovation statistics. For this study, we used the fixed perturbation length scales from Caya et al. (2005), and we chose the magnitudes of the additive noise through experimentation. Length scales representative of initial analysis uncertainty and later forecast errors could be significantly different, but the current method does not account for such a difference. In future studies, an adaptive method with situation-dependent perturbation magnitudes and length scales (Mitchell and Houtekamer 2000) based on Doppler velocity innovation statistics could be developed. However, without thermodynamic observations available on the storm scale, tuning ensemble spread in the thermodynamic fields remains somewhat ad hoc.

It might be possible to develop an improved covariance-inflation method that takes advantage of the same information that the additive-noise method is provided. That is, a local inflation method could be developed that increases ensemble spread where reflectivity is high and does not modify the ensemble where the reflectivity is low. Spatially and temporally varying inflation has proven helpful for other applications (Anderson 2009). The additive-noise technique proposed here provides more flexibility for tuning assimilation results than does an inflation method, which could be both an advantage and a disadvantage. Perhaps more importantly, the additive-noise technique has the potential to produce ensembles that span a more diverse subspace than ensembles modified through inflation. For example, when the numerical model fails to capture the initial

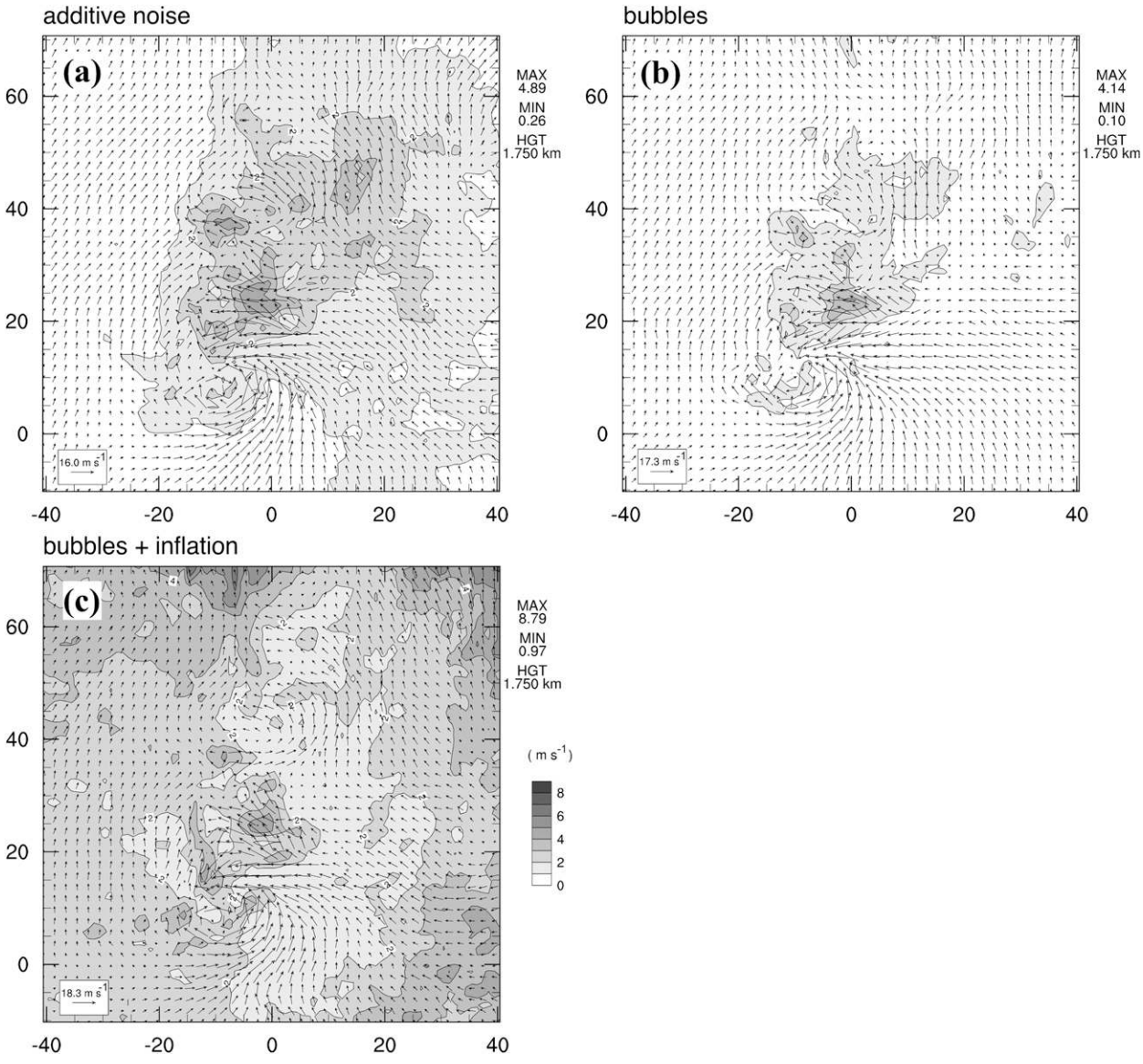

FIG. 11. Ensemble standard deviation of the v wind component (contours and shading at intervals of 1 m s^{-1}) and ensemble-mean horizontal winds (vectors) at 1750 m AGL at 2208 UTC. (a) Experiment with additive noise (0.25 m s^{-1} and 0.25 K) throughout the assimilation window. (b) Experiment initialized with warm bubbles. (c) Experiment initialized with warm bubbles and with covariance inflation throughout the assimilation window.

development of a new convective storm with precipitation, the additive-noise technique responds by increasing ensemble spread there, providing the ensemble an opportunity to recover during the subsequent forecast and data-assimilation cycles.

We are currently applying the additive-noise technique to a variety of convective storm cases, employing simplified environmental conditions, and will report on the results in later papers. In the near future, we also plan to implement the method in a mesoscale model with full complexity. Our intent is to use mesoscale ensemble techniques to represent environmental variability and uncertainty while using the additive-noise method to maintain ensemble spread within the convective storms.

In future studies, the additive-noise technique could employ other observation types and/or be applied on larger scales. For example, one of the challenges for storm-scale radar data assimilation is how long it takes to identify the locations of new convective storms; reflectivity and Doppler velocity observations typically do not become available until precipitation develops, which can occur up to a few tens of minutes after initial cloud development. Satellite observations could identify

convective cloud formation, and thus locations where ensemble perturbations are needed, sooner than radar observations. Finally, the additive noise used for storm-scale data assimilation in the current study is localized. We infer from the work of Houtekamer and Mitchell (2005) and Hamill and Whitaker (2005) that using flow-dependent (e.g., localized) additive noise could also prove useful for larger-scale applications.

Acknowledgments. This work began while the lead author was supported by the National Science Foundation under ATM-0333872 at the Cooperative Institute for Mesoscale Meteorological Studies and was completed at the National Center for Atmospheric Research. Matt Gilmore developed the precipitation-microphysics scheme used in these experiments and answered questions about the code. Mike Coniglio, Ted Mansell, and Glen Romine contributed to the data-assimilation code development. Chris Snyder, Ted Mansell, and two anonymous reviewers provided helpful comments on the manuscript. Discussions with Alain Caya and Altug Aksoy were also quite helpful. Kevin Scharfenberg and Gordon Carrie provided the radar observations of the 8 May 2003 Oklahoma City supercell. Mary Haley provided helpful assistance with NCL graphics.

REFERENCES

Aksoy, A., D. C. Dowell, and C. Snyder, 2009: A multicase comparative assessment of the ensemble Kalman filter for assimilation of radar observations. Part I: Storm-scale analyses. *Mon. Wea. Rev.,* in press.

Anderson, J. L., 2001: An ensemble adjustment Kalman filter for data assimilation. *Mon. Wea. Rev.,* **129,** 2884–2903.

——, 2009: Spatially- and temporally-varying adaptive covariance inflation for ensemble filters. *Tellus,* **61,** 72–83.

——, and S. L. Anderson, 1999: A Monte Carlo implementation of the nonlinear filtering problem to produce ensemble assimilations and forecasts. *Mon. Wea. Rev.,* **127,** 2741–2758.

Browning, K. A., 1964: Airflow and precipitation trajectories within severe local storms which travel to the right of the winds. *J. Atmos. Sci.,* **21,** 634–639.

Buizza, R., P. L. Houtekamer, Z. Toth, G. Pellerin, M. Wei, and Y. Zhu, 2005: A comparison of the ECMWF, MSC, and NCEP global ensemble prediction systems. *Mon. Wea. Rev.,* **133,** 1076–1097.

Burgess, D. W., 2004: High resolution analyses of the 8 May 2003 Oklahoma City storm. Part I: Storm structure and evolution from radar data. Preprints, *22nd Conf. on Severe Local Storms*, Hyannis, MA, Amer. Meteor. Soc., 12.4. [Available online at http://ams.confex.com/ams/pdfpapers/81939.pdf.]

Caya, A., J. Sun, and C. Snyder, 2005: A comparison between the 4DVAR and the ensemble Kalman filter techniques for radar data assimilation. *Mon. Wea. Rev.,* **133,** 3081–3094.

Coniglio, M. C., D. J. Stensrud, and L. J. Wicker, 2006: Effects of upper-level shear on the structure and maintenance of strong quasi-linear mesoscale convective systems. *J. Atmos. Sci.,* **63,** 1231–1252.

Dee, D. P., and A. M. da Silva, 1998: Data assimilation in the presence of forecast bias. *Quart. J. Roy. Meteor. Soc.,* **124,** 269–295.

Dowell, D. C., F. Zhang, L. J. Wicker, C. Snyder, and N. A. Crook, 2004a: Wind and temperature retrievals in the 17 May 1981 Arcadia, Oklahoma, supercell: Ensemble Kalman filter experiments. *Mon. Wea. Rev.,* **132,** 1982–2005.

——, L. J. Wicker, and D. J. Stensrud, 2004b: High resolution analyses of the 8 May 2003 Oklahoma City storm. Part II: EnKF data assimilation and forecast experiments. Preprints, *22nd Conf. on Severe Local Storms*, Hyannis, MA, Amer. Meteor. Soc., 12.5. [Available online at http://ams.confex.com/ams/pdfpapers/81393.pdf.]

Eckel, F. A., and C. F. Mass, 2005: Aspects of effective mesoscale, short-range ensemble forecasting. *Wea. Forecasting,* **20,** 328–350.

Evensen, G., 1994: Sequential data assimilation with a nonlinear quasi-geostrophic model using Monte Carlo methods to forecast error statistics. *J. Geophys. Res.,* **99** (C5), 10 143–10 162.

Fujita, T., D. J. Stensrud, and D. C. Dowell, 2007: Surface data assimilation using an ensemble Kalman filter approach with initial condition and model physics uncertainties. *Mon. Wea. Rev.,* **135,** 1846–1868.

Gaspari, G., and S. E. Cohn, 1999: Construction of correlation functions in two and three dimensions. *Quart. J. Roy. Meteor. Soc.,* **125,** 723–757.

Gilmore, M. S., J. M. Straka, and E. N. Rasmussen, 2004: Precipitation and evolution sensitivity in simulated deep convective storms: Comparisons between liquid-only and simple ice and liquid phase microphysics. *Mon. Wea. Rev.,* **132,** 1897–1916.

Hamill, T. M., and J. S. Whitaker, 2005: Accounting for the error due to unresolved scales in ensemble data assimilation: A comparison of different approaches. *Mon. Wea. Rev.,* **133,** 3132–3147.

——, ——, and C. Snyder, 2001: Distance-dependent filtering of background error covariance estimates in an ensemble Kalman filter. *Mon. Wea. Rev.,* **129,** 2776–2790.

Houtekamer, P. L., and H. L. Mitchell, 1998: Data assimilation using an ensemble Kalman filter technique. *Mon. Wea. Rev.,* **126,** 796–811.

——, and ——, 2001: A sequential ensemble Kalman filter for atmospheric data assimilation. *Mon. Wea. Rev.,* **129,** 123–137.

——, and ——, 2005: Ensemble Kalman filtering. *Quart. J. Roy. Meteor. Soc.,* **131,** 3269–3289.

Jazwinski, A. H., 1970: *Stochastic Processes and Filtering Theory*. Academic Press, 376 pp.

Klemp, J. B., and R. B. Wilhelmson, 1978: The simulation of three-dimensional convective storm dynamics. *J. Atmos. Sci.,* **35,** 1070–1096.

Lemon, L. R., and C. A. Doswell III, 1979: Severe thunderstorm evolution and mesocyclone structure as related to tornadogenesis. *Mon. Wea. Rev.,* **107,** 1184–1197.

Lin, Y.-L., R. D. Farley, and H. D. Orville, 1983: Bulk parameterization of the snow field in a cloud model. *J. Climate Appl. Meteor.,* **22,** 1065–1092.

Mitchell, H. L., and P. L. Houtekamer, 2000: An adaptive ensemble Kalman filter. *Mon. Wea. Rev.,* **128,** 416–433.

Romine, G. S., D. W. Burgess, and R. B. Wilhelmson, 2008: A dual-polarization-radar-based assessment of the 8 May 2003 Oklahoma City area tornadic supercell. *Mon. Wea. Rev.,* **136,** 2849–2870.

Smith, P. L., 1984: Equivalent radar reflectivity factors for snow and ice particles. *J. Appl. Meteor.,* **23,** 1258–1260.

——, C. G. Myers, and H. D. Orville, 1975: Radar reflectivity factor calculations in numerical cloud models using bulk parameterization of precipitation. *J. Appl. Meteor.,* **14,** 1156–1165.

Snyder, C., and F. Zhang, 2003: Assimilation of simulated Doppler radar observations with an ensemble Kalman filter. *Mon. Wea. Rev.,* **131,** 1663–1677.

Stensrud, D. J., H. E. Brooks, J. Du, M. S. Tracton, and E. Rogers, 1999: Using ensembles for short-range forecasting. *Mon. Wea. Rev.,* **127,** 433–446.

Sun, J., and N. A. Crook, 2001: Real-time low-level wind and temperature analysis using single WSR-88D data. *Wea. Forecasting,* **16,** 117–132.

Tong, M., and M. Xue, 2005: Ensemble Kalman filter assimilation of Doppler radar data with a compressible nonhydrostatic model: OSS experiments. *Mon. Wea. Rev.,* **133,** 1789–1807.

Whitaker, J. S., and T. M. Hamill, 2002: Ensemble data assimilation without perturbed observations. *Mon. Wea. Rev.,* **130,** 1913–1924.

Wicker, L. J., and W. C. Skamarock, 2002: Time-splitting methods for elastic models using forward time schemes. *Mon. Wea. Rev.,* **130,** 2088–2097.

Zhang, F., C. Snyder, and J. Sun, 2004: Impacts of initial estimate and observations on convective-scale data assimilation with an ensemble Kalman filter. *Mon. Wea. Rev.,* **132,** 1238–1253.